AIAA JOURNAL
Vol. 48, No. 7, July 2010

Jet Noise: Acoustic Analogy Informed by Large Eddy Simulation

S. A. Karabasov,* M. Z. Afsar,† T. P. Hynes,‡ and A. P. Dowling§
University of Cambridge, Cambridge, England CB2 1TN, United Kingdom
and
W. A. McMullan,¶ C. D. Pokora,** G. J. Page,†† and J. J. McGuirk‡‡
Loughborough University, Loughborough, England LE11 3TU, United Kingdom

DOI: 10.2514/1.44689

A novel approach to the development of a hybrid prediction methodology for jet noise is described. Modeling details and numerical techniques are optimized for each of the three components of the model. Far-field propagation is modeled by solution of a system of adjoint linear Euler equations, capturing convective and refraction effects using a spatially developing jet mean flow provided by a Reynolds-averaged Navier–Stokes computational fluid dynamics solution. Sound generation is modeled following Goldstein's acoustic analogy, including a Gaussian function model for the two-point cross correlation of the fourth-order velocity fluctuations in the acoustic source. Parameters in this model describing turbulent length and time scales are assumed to be proportional to turbulence information also taken from the Reynolds-averaged Navier–Stokes computational fluid dynamics prediction. The constants of proportionality are, however, not determined empirically, but extracted by comparison with turbulence length and time scales obtained from a large eddy simulation prediction. The large eddy simulation results are shown to be in good agreement with experimental data for the fourth-order two-point cross-correlation functions. The large eddy simulation solution is then used to determine the amplitude parameter and also to examine which components of the cross correlation are largest, enabling inclusion of all identified dominant terms in the Gaussian source model. The acoustic source description in the present approach is therefore determined with no direct input from experimental data. This model is applied to the prediction of sound to the experimental configuration of the European Union JEAN project, and gives encouraging agreement with experimental data across a wide spectral range and for both sideline and peak noise angles. This paper also examines the accuracy of various commonly made simplifications, for example: a locally parallel mean flow approximation rather than consideration of the spatially evolving mean jet flow and scattering from the nozzle; the assumption of small radial variation in Green function over the turbulence correlation length; the application of the far-field approximation in the Green function; and the impact of isotropic assumptions made in previous acoustic source models.

I. Introduction

DEVELOPMENTS of the original acoustic analogy proposed by Lighthill [1] remain a major tool for the prediction of jet noise. By an exact rearrangement of the Navier–Stokes equations, Lighthill [1] showed that the noise from a turbulent jet could be viewed as a distribution of quadrupole sources in the acoustic wave equation, the strength of the quadrupoles, T_{ij}, depending primarily on the local fluctuating Reynolds stresses. The turbulent eddies which give rise to the Reynolds stresses are convected by the jet velocity and their motion alters the radiated sound, an effect correctly accounted for by Ffowcs Williams [2]. The mean jet velocity has yet another influence: it refracts the sound [3,4] altering the propagation of sound from the sources to the far field. Lilley's approach [5] was to describe this propagation through a specified mean-flow velocity profile, taken to be a function of radius only. This is clearly restrictive, introducing sensitivity to the axial station chosen for matching the velocity profile [6].

Goldstein's generalized acoustic analogy [7] rearranges the Navier–Stokes equations into linearized Euler equations (LEE) (involving the spatially developing mean jet flow) for the propagating quantities, with nonlinear terms representing the analogous acoustic sources. This formulation provides a consistent framework in which the convection effects on acoustic sources and the refraction effects on the sound can be correctly captured if the true evolving mean jet flow is used.

Goldstein's formulation has been used in some previous studies. For example, it was considered by Samanta et al. [8], among other popular acoustic analogy formulations, for a 2D shear-layer problem in conjunction with the complete direct numerical simulation (DNS) data. This work showed that all acoustic analogies lead to the same numerical sound integral if the full DNS solution is used for acoustic source modeling but Goldstein's formulation appears to be the most robust when numerical errors are introduced in the DNS solution. More recently, Goldstein and Leib [9] extended Goldstein's formulation to successfully predict jet noise from 3D high-speed subsonic and moderately supersonic jets. In their work a weakly nonparallel flow model was developed to eliminate the critical layer singularity produced by the mean-flow Doppler factor that produces a uniformly valid solution everywhere in the flow.

In the current work, a complete mean-flow propagation jet model is implemented for both large and small observation angles to the jet. The sound field is represented using an adjoint Green function solution [10] of the LEE together with a model or calculation of the statistics of the source terms [8]. Because the LEEs are also those

Presented as Paper 2985 at the 14th AIAA/CEAS Aeroacoustics Conference (29th AIAA Aeroacoustics Conference), Vancouver, British Columbia, 5–7 May 2008; received 1 April 2009; revision received 16 February 2010; accepted for publication 15 March 2010.

*Royal Society University Research Fellow, Department of Engineering. Member AIAA.
†Ph.D. Student, Department of Engineering. Student Member AIAA.
‡Reader in Mechanical Engineering, Department of Engineering. Member AIAA.
§Professor of Mechanical Engineering, Department of Engineering. Member AIAA.
¶Postdoctoral Research Associate, Department of Aeronautical and Automotive Engineering.
**Ph.D. Student, Department of Aeronautical and Automotive Engineering.
††Senior Lecturer, Department of Aeronautical and Automotive Engineering. Member AIAA.
‡‡Professor of Aerodynamics, Department of Aeronautical and Automotive Engineering.

which govern shear flow instability, it is important, as pointed out by Argawal et al. [11], to avoid contamination by shear flow instabilities. This can be accomplished by solving the LEE in the frequency domain provided the method of iteration is carefully chosen [12].

In a number of previous investigations of jet noise [13,14], a statistically stationary Reynolds-averaged Navier–Stokes (RANS) solution for the jet flowfield, incorporating a k-ε turbulence model, has been used to determine the underlying mean flow, and to provide statistical (time-averaged) turbulence information which was used to characterize the acoustic sources. The two-point space-time correlation function of the acoustic sources was estimated via an assumed model function, whose amplitude and integral length and time scales were deduced from the predicted turbulence information via empirically determined relationships. Tam and Auriault [14] introduced a model through a heuristic argument based on an analogy between molecular pressure, from the kinetic theory of gases, and the turbulent pressure from fine-scale turbulence. Morris and Farassat [15] showed this to be equivalent to an acoustic analogy provided one represents the source and Green function consistently.

Sound predictions based upon source statistics derived from RANS calculations under the assumption that the turbulent Reynolds stresses, T_{ij}, are isotropic everywhere and at all times give good predictions of the higher frequency sound that dominates at 90° to the jet axis (the important sideline condition in aircraft certification) and in the forward arc [14]. However, this approach gives a significant under prediction in the rearward arc, where sound is of lower frequency and comes from larger-scale coherent structures in the jet [15]. Afsar et al. [16] argued that a more realistic model of this type would be to assume that the turbulence is only statistically isotropic, i.e., that the temporal-spatial (two-time, two-point) cross correlation of the turbulent sources is isotropic rather than T_{ij}, itself. By using the quasi-normal axisymmetric model of turbulent acoustic sources based on the RANS statistics and empirical fits to the experiment-derived integral space and time scales Goldstein and Leib [9] obtained good far-field sound predictions for a wide range of frequencies and observer angles for several high-speed axisymmetric jet cases.

The turbulent statistics associated with large-scale coherent structures, potentially contributing to low-frequency sound, appear amenable to calculation by more advanced methods. In this paper we will use large eddy simulation (LES) CFD of a jet to generate these. By comparison with those obtained from RANS CFD, we aim to develop better source models, which rely on less empiricism for correlation scales and which are valid for a much wider range of frequencies.

The methodology proposed here may be summarized as follows:

1) Acoustic propagation is handled using a Goldstein decomposition and an efficient solution of the LEEs using an adjoint method.

2) The input needed for solution of the LEE system is extracted from a mix of CFD models, balancing computational affordability and ability to predict different aspects of the flow and turbulence structure.

3) The time-averaged flowfield is taken from a RANS CFD solution using a k-ε turbulence model.

The acoustic source terms are informed by LES CFD solution, specifically:

1) The nondimensional shapes of the fourth-order two-point two-time correlations of the turbulent Reynolds stresses R_{ijkl} are determined by fitting to LES predicted correlations.

2) The time and length scales used in the nondimensional R_{ijkl} are, at each point in the flowfield, extracted from RANS k-ε predictions but with proportionality constants fitted to time/length scales extracted from LES predictions.

3) The relative amplitudes of individual R_{ijkl} components are extracted from LES predictions.

In Sec. II, we describe the acoustic analogy, source representation theorem and Green function method. Section III provides a description of the LES method and its comparison with experimental data, together with the prediction of acoustic source statistics. Models of these statistics are developed in Sec. IV and used to infer the far-field sound that is compared with experiment.

II. Representation of Acoustic Field

Following Goldstein [7], we decompose the flow variables for density, pressure, velocity and enthalpy into a steady mean and unsteady perturbation of the form

$$\rho = \bar{\rho} + \rho' \qquad p = \bar{p} + p' \qquad v_i = \tilde{v}_i + v_i'' \qquad h = \tilde{h} + h''$$

where $\overline{(\,)}$ represents a time average, $\widetilde{(\,)}$ a Favre average and single and double primes represent the corresponding variation about the mean. The unsteady Navier–Stokes equations can then be rearranged into linearized Euler terms on the left hand side operating on perturbation variables equal to simple nonlinear source terms on the right. These are, with position and time represented by $(\mathbf{y}, \tau)$

$$\frac{\partial \rho'}{\partial \tau} + \frac{\partial}{\partial y_j}(\rho' \tilde{v}_j + u_j) = 0$$

$$\frac{\partial u_i}{\partial \tau} + \frac{\partial}{\partial y_j}(\tilde{v}_j u_i) + \frac{\partial p'}{\partial y_i} + u_j \frac{\partial \tilde{v}_i}{\partial y_j} - \left(\frac{\rho'}{\bar{\rho}}\right)\frac{\partial \tilde{\tau}_{ij}}{\partial y_j} = \frac{\partial T'_{ij}}{\partial y_j} \qquad i = 1, ..3.$$

$$\left(\frac{1}{\gamma - 1}\right)\frac{\partial p'}{\partial \tau} + \left(\frac{1}{\gamma - 1}\right)\frac{\partial}{\partial y_j}(p' \tilde{v}_j) + \frac{\partial}{\partial y_j}(u_j \tilde{h}) + p' \frac{\partial \tilde{v}_j}{\partial y_j} - \left(\frac{u_i}{\bar{\rho}}\right)\frac{\partial \tilde{\tau}_{ij}}{\partial y_j} = Q \tag{1}$$

In this formulation, a momentum pertubation variable is defined (with zero time average) as $u_i = \rho v_i''$, and the Favre-averaged stagnation enthalpy, and its perturbation, take the special definitions

$$\tilde{h}_o = \tilde{h} + \frac{1}{2}\tilde{v}^2 \quad \text{and} \quad h_o'' = h'' + \tilde{v}_i v_i'' + \frac{1}{2} v''^2 \tag{2}$$

The source terms are

$$T'_{ij} = -(\rho v_i'' v_j'' - \bar{\rho}\,\widetilde{v_i'' v_j''}) \tag{3}$$

$$Q = -\tilde{v}_j \frac{\partial T'_{ij}}{\partial y_i} + \frac{1}{2}\delta_{ij}\left[\frac{DT'_{ij}}{D\tau} + \frac{\partial \tilde{v}_k}{\partial y_k} T'_{ij}\right] - \frac{\partial}{\partial y_j}(\rho v_j'' h_o'' - \bar{\rho}\,\widetilde{v_j'' h_o''}) \tag{4}$$

where $D/D\tau$ is the convective derivative, $\frac{D}{D\tau} = \frac{\partial}{\partial \tau} + \tilde{v}_j(\mathbf{y})\frac{\partial}{\partial y_j}$.

For the unheated jets considered in this paper, we will assume that the last term in Eq. (4) is negligible. With this approximation, Q reduces to

$$Q = -\tilde{v}_j \frac{\partial T'_{ij}}{\partial y_i} + \frac{1}{2}\delta_{ij}\left[\frac{DT'_{ij}}{D\tau} + \frac{\partial \tilde{v}_k}{\partial y_k} T'_{ij}\right] \tag{5}$$

The wave propagation problem is solved in the frequency domain using an adjoint Green function method. $\hat{\mathbf{G}}(\mathbf{y}, \omega|\mathbf{x})$, the Fourier transform of the adjoint Green function, satisfies the adjoint equations:

$$i\omega \hat{G}_o + \tilde{v}_j \frac{\partial \hat{G}_o}{\partial y_j} + \left(\frac{\hat{G}_i}{\bar{\rho}}\right)\frac{\partial \tilde{\tau}_{ij}}{\partial y_j} = 0$$

$$i\omega \hat{G}_j + \frac{\partial \hat{G}_o}{\partial y_j} + \tilde{v}_i \frac{\partial \hat{G}_j}{\partial y_i} - \hat{G}_i \frac{\partial \tilde{v}_i}{\partial y_j} + \tilde{h}\frac{\partial \hat{G}_4}{\partial y_j} + \left(\frac{\hat{G}_4}{\bar{\rho}}\right)\frac{\partial \tilde{\tau}_{ij}}{\partial y_i} = 0 \qquad j = 1, ..3.$$

$$\left(\frac{i\omega}{\gamma - 1}\right)\hat{G}_4 + \left(\frac{\tilde{v}_j}{\gamma - 1}\right)\frac{\partial \hat{G}_4}{\partial y_j} - \hat{G}_4 \frac{\partial \tilde{v}_j}{\partial y_j} + \frac{\partial \hat{G}_j}{\partial y_j} = \delta(\mathbf{y} - \mathbf{x}) \tag{6}$$

In the adjoint formulation, the unit point source in Eq. (6) is at $\mathbf{x}$, the position of the observer, and is generally at some distance from the jet. $\hat{G}_o$ is the adjoint density-like variable and $\hat{G}_1$-$\hat{G}_3$ are the adjoint momentum-like variables. $\hat{G}_4$, the pressure-like quantity, is the variable in the adjoint energy equation.

For axisymmetric jets, it is convenient to express $\hat{\mathbf{G}}$ as the sum of a free-space solution for a point source at $\mathbf{x}$ (which is known analytically) and a scattered field due to the presence of the jet in the manner of Tam and Auriault [8]

$$\hat{\mathbf{G}} = \hat{\mathbf{G}}_{\text{free-space}} + \hat{\mathbf{G}}_{\text{scattered}} \tag{7}$$

The scattered field is found in the frequency domain as a sum of circumferential harmonics by numerical solution of Eq. (6), for each harmonic, using a finite volume version of a modified Adams scheme. As described by Argawal et al. [11], the linearized Euler equations are those governing the growth of jet shear-layer instability in addition to sound propagation and it is important that the solution obtained for the Green function does not contain any part of the shear-layer instability solution. Accordingly, the convergence to the frequency domain solution is achieved through a carefully adjusted dual-scale iterative pseudotime stepping scheme to stabilize the effects of large shear gradient terms and to avoid contamination by the shear-layer instability [12].

The iterative time steps are specially adjusted so that the most unstable eigenvalues of the spatially discretized propagation operator are shifted to the stable part of the numerical solution plane. The dual-scale iterative pseudotime stepping scheme is equivalent to introducing a new preconditioner/rescaling procedure that is specifically tailored for the governing elliptic system of algebraic equations. This preconditioner allows us to suppress those eigensolutions of the propagator which do not satisfy the additional physical constraint of the partial solution of the boundary-value problem, i.e., solution boundedness, and correspond to the spurious shear-layer instability waves. A systematic description of the new algorithm will be the subject of a future publication. In the present paper we include one example showing the application of the new LEE method for solving a benchmark problem from the fourth Computational Aeroacoustics Workshop that was discussed in Argawal et al. [11]. In the benchmark problem a monopole Gaussian source is specified at $(x, y) = 0$ on the symmetry plane of a 2D parallel shear flow with characteristic width $\Delta y = 1.3$ and pulsates at a frequency that corresponds to the shear-layer instability. The full LEE solution consists of the refracted acoustic wave and the Kelvin–Helmholtz instability wave and the benchmark challenge is to obtain the solution of the LEE that corresponds to the acoustic solution without any instability wave. Figure 1 shows the comparison with the analytic solution along the line $y = 15$ and the spatial distribution of the converged LEE solution that contains only the acoustic component.

When the observer position $\mathbf{x}$ is at a large distance from the jet, the spatial dependence of $\hat{\mathbf{G}}_{\text{free-space}}$ on $\mathbf{y}$ takes the form of the n'th circumferential harmonic of a plane wave [10]. For comparison with the experiments that are described in Sec. IV, where the acoustic measurements were taken at 30 diameters from the jet, the spatial dependence of $\hat{\mathbf{G}}_{\text{free-space}}$ includes the next term in $\sigma/|\mathbf{x}|$, where σ is the radial component of $\mathbf{y}$ [12].

The underlying mean flow for the linearized solution was extracted from a RANS solution on a carefully chosen mesh. The solution domain includes the nozzle and is terminated at a large downstream distance using a sponge zone [12]. The boundary condition on $\hat{\mathbf{G}}$ at large distances from the jet is chosen to ensure that no surface terms appear in the representation formula for the desired flow variables.

It is relatively straightforward to formulate a representation theorem for the far-field pressure in terms of the Green function and source terms. The sum of the inner products of $\hat{\mathbf{G}}$ with Eq. (1) and the perturbation variables with Eq. (6) is integrated over the region of nonzero sources. The expression obtained for the far-field pressure is

$$\hat{p}(\mathbf{x},\omega) = -\int_{V_\infty(\mathbf{y})} \left(\hat{G}_i(\mathbf{y}, -\omega|\mathbf{x}) \frac{\partial \hat{T}'_{ij}}{\partial y_j}(\mathbf{y},\omega) + \hat{G}_4(\mathbf{y}, -\omega|\mathbf{x}) \hat{Q}(\mathbf{y},\omega) \right) \mathrm{d}^3\mathbf{y} \tag{8}$$

where $\hat{T}'_{ij}(\mathbf{y},\omega)$ and $\hat{Q}(\mathbf{y},\omega)$ are the Fourier transform of the source terms. After expanding $\hat{Q}(\mathbf{y},\omega)$ as in Eq. (5) and integration by parts, we obtain

$$\hat{p}(\mathbf{x},\omega) = \int_{V_\infty(\mathbf{y})} \hat{I}_{ij}(\mathbf{y}, -\omega|\mathbf{x}) \hat{T}'_{ij}(\mathbf{y},\omega)\, \mathrm{d}^3\mathbf{y} \tag{9}$$

where the components of the second rank wave propagation tensor, $\hat{I}_{ij}$, are defined by

$$\hat{I}_{ij}(\mathbf{y},\omega|\mathbf{x}) = \frac{\partial \hat{G}_j}{\partial y_i}(\mathbf{y},\omega|\mathbf{x}) - \left[\frac{\partial \tilde{v}_j}{\partial y_i}(\mathbf{y}) \hat{G}_4(\mathbf{y},\omega|\mathbf{x}) + \tilde{v}_j(\mathbf{y}) \frac{\partial \hat{G}_4}{\partial y_i}(\mathbf{y},\omega|\mathbf{x}) \right] + \frac{\delta_{ij}}{2} \left(i\omega + \tilde{v}_k \frac{\partial}{\partial y_k} \right) \hat{G}_4(\mathbf{y},\omega|\mathbf{x}) \tag{10}$$

Finally, the power spectral density of the distant sound field

$$\hat{P}(\mathbf{x},\omega) = \int_{V_\infty(\mathbf{y})} \int_{\boldsymbol{\Delta}} \hat{R}_{ijkl}(\mathbf{y},\boldsymbol{\Delta},\omega) \hat{I}_{ij}(\mathbf{y},\omega|\mathbf{x}) \hat{I}_{kl} \times (\mathbf{y}+\boldsymbol{\Delta}, -\omega|\mathbf{x})\, \mathrm{d}^3\boldsymbol{\Delta}\, \mathrm{d}^3\mathbf{y} \tag{11}$$

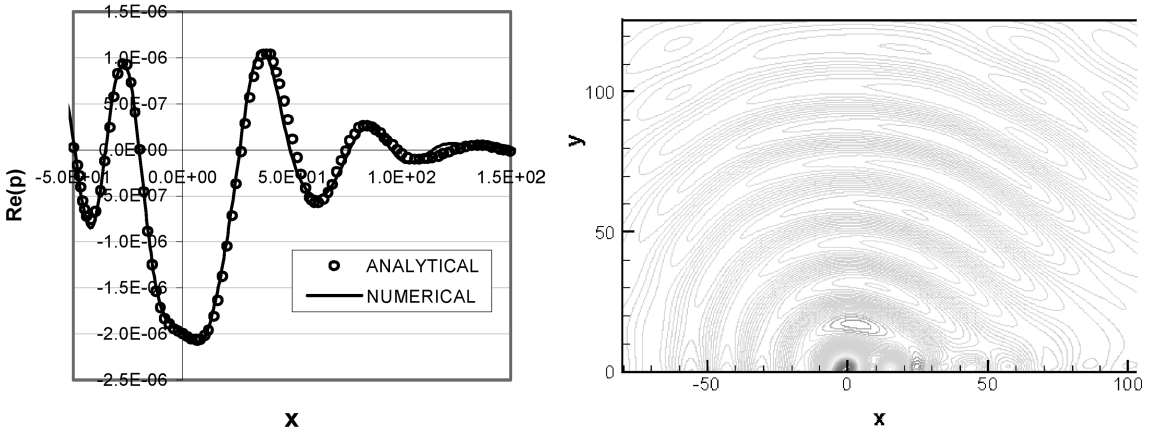

Fig. 1 Numerical LEE solution to the fourth computational aeroacoustics benchmark problem of sound propagation from a point source through a 2D shear-layer, pressure fluctuation amplitude: a) comparison with the analytic solution, and b) 2D contour lines of the converged LEE solution.

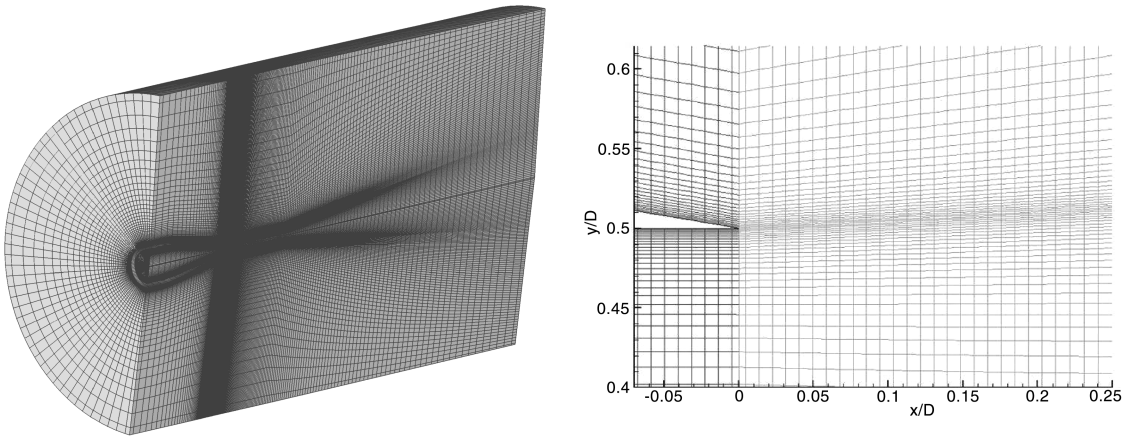

Fig. 2 Mesh distribution: whole domain and near the nozzle lip for the LES case.

where $\hat{R}_{ijkl}(\mathbf{y}, \boldsymbol{\Delta}, \omega)$ is the Fourier transform of the temporal-spatial (two-time, two-point) cross correlation of the turbulent sources:

$$\hat{R}_{ijkl}(\mathbf{y}, \boldsymbol{\Delta}, \omega) = \int R_{ijkl}(\mathbf{y}, \boldsymbol{\Delta}, \tau) e^{-i\omega\tau} \, \mathrm{d}\tau$$
$$= \int \overline{T'_{ij}(\mathbf{y}, t) T'_{kl}(\mathbf{y} + \boldsymbol{\Delta}, t + \tau)} e^{-i\omega\tau} \, \mathrm{d}\tau \tag{12}$$

III. LES/RANS Modeling

The governing Navier–Stokes equations are spatially filtered to give the LES form, which then requires a subgrid scale model to define the unknown subgrid scale stresses. The equations are solved using a finite volume cell-centered spatial discretization on hexahedral elements. The elements are defined using a structured mesh multiblock formulation. This allows the capture of reasonably complex geometry (for example engine pylons or chevrons) while being computationally efficient.

The spatial discretization is implemented as a family of schemes ranging from central differencing through first order upwind to high-order upwind, with a single controlling parameter. In this work a second-order upwind scheme is used as a compromise between numerical robustness and acceptable dispersion and dissipation characteristics. Whilst a fourth-order or greater spatial discretization would be preferable, for example, as used by Bogey and Bailly [17]; for jet noise prediction the finite volume meshes needed to handle realistic geometry such as nozzles, pylons or chevrons means that spatial orders of accuracy greater than two are difficult to achieve in practice. Many workers have carried out successful large eddy simulations of jet noise using similar high-order upwind schemes to the current work [18]. The generic upwind scheme is applied to the mass, momentum and energy equations. These equations are solved in a sequential manner with a spatially implicit scheme. The mass equation is transformed into an equation for pressure-correction. This allows the computation of both compressible and low-speed incompressible flows without extra numerical treatments such as preconditioning. Temporal advancement is by a first-order backward Euler implicit scheme or a low-storage Runge–Kutta third-order (three stage) or fourth-order (five stage) scheme. The subgrid scale model used is the standard Smagorinsky formulation with a Van Driest damping treatment to limit the length scale in the high aspect ratio cells in the near wall viscous affected region. Further details of the methodology are provided in McMullan et al. [19].

The baseline methodology has been tested for steady state RANS solutions for both high-speed compressible flows with shock waves, and low-speed incompressible problems (Page et al. [20]). The LES capability was originally developed for the prediction of multiple impinging jets (Page et al. [21]). The use of a multiblock formulation means that the algorithm is easily amenable to parallelization in both shared memory or message passing formulations. These calculations were run with each block allocated to a single processor on an MPI based compute cluster.

The 3D computational grid used in the LES calculations has a total of 17 million cells and has an extent of $30D \times 10D$ in the axial and radial directions downstream of the nozzle exit of diameter D. The jet nozzle wall geometry is included in the domain and extends $5D$ upstream of the nozzle exit. 2.4 million cells, separated into two blocks, are located inside the nozzle, with the grid refined near the nozzle walls to produce a first cell height of $y + \sim 30$. A further 2.6 million cells are placed in the region between the outer wall of the nozzle and the computational domain boundary upstream of the nozzle exit. At the nozzle lip, the axial grid spacing is $0.0045D$, the radial spacing is $0.004D$ and the azimuthal 1 ° spacing is $0.0087D$; thus the grid aspect ratios in this crucial area are of order unity. Images of the mesh, including a closeup around the nozzle exit are

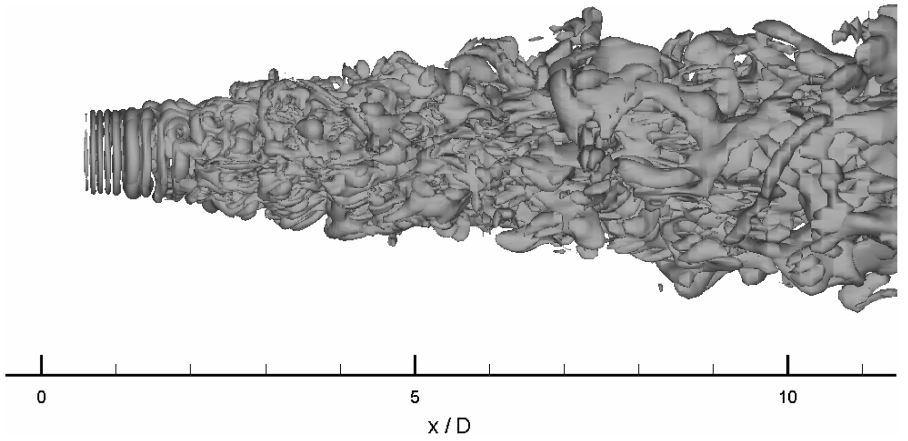

Fig. 3 LES predicted instantaneous isosurface of vorticity.

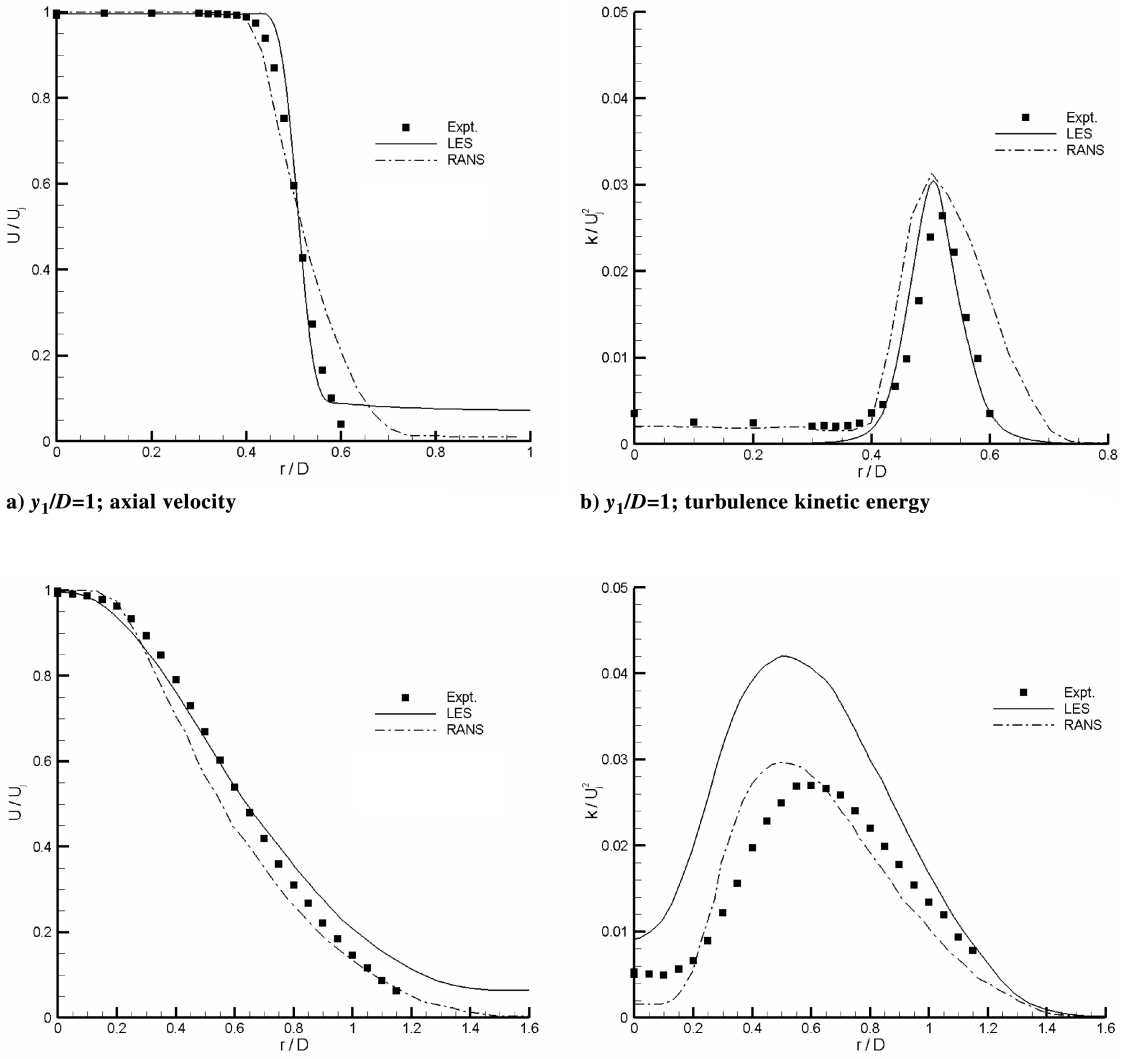

a) y_1/D=1; axial velocity

b) y_1/D=1; turbulence kinetic energy

c) y_1/D=5; axial velocity

d) y_1/D=5; turbulence kinetic energy

Fig. 4 Radial profiles of axial velocity and turbulence kinetic energy from Power et al. [22].

shown in Fig. 2, which also indicates the mesh design to provide high resolution in the jet shear-layer region. Downstream of the nozzle exit, the $314 \times 102 \times 360$ grid (axial x radial x circumferential) is partitioned into seven blocks, sliced normal to the jet axis.

The simulated flow is an isothermal Mach 0.75 round jet with a Reynolds number of 10^6, based on the jet exit velocity and the nozzle diameter (based on Power et al. [22]). A constant total pressure condition is specified at nozzle inlet to set the correct jet Reynolds and Mach numbers. A fixed static pressure outlet condition at the downstream boundary and far-field radiation boundaries with a stretched grid are used in the LES calculations. For the LES prediction, the nozzle inlet flow has Gaussian random noise applied to the velocity field equivalent to a turbulence level of 10%. As the code is finite volume cell-center based, the singularity along the jet centerline does not require any special treatment. Because of the uncorrelated nature of this disturbance and the acceleration in the nozzle, this rapidly decays to very low levels in the potential core of the jet. The Smagorinsky model coefficient (C_S) is set to 0.15, and we have found little sensitivity of the solution to the value of this coefficient. The time step of the simulation is 1.4×10^{-3} in units nondimensionalized by jet velocity and diameter, approximately 700 time steps are required for a parcel of fluid at the jet exit velocity to travel one jet diameter downstream. The LES simulation is first run for 100,000 time steps using the backward Euler temporal scheme, so that the initial conditions have passed through the domain and a statistically stationary flow-field is obtained. To gather statistical data and information required to produce the second- and fourth-order velocity correlations, the simulation is then run for a further 100,000 time steps; during this time the entire flow-field is sampled at intervals of 40 LES time steps. Within each 40 time step window, a filter is applied that is designed to attenuate fluctuations with two or less subsamples per wavelength. The file-size of the filtered flow solution at each time step is ~450 MB, and up to 1 TB of data is produced by the sampling procedure, rendering the extraction, processing and construction of two-point two-time correlations from the stored data very time-consuming, requiring perhaps days of computational effort in its own right.

The RANS solution was obtained using the commercial CFD product Fluent 6.2 (k-ε model with default parameters and a second-order upwind coupled explicit solver). This calculation is performed on a different grid with 271×120 cells (axial $\times$ radial) and had a somewhat smaller domain of $20D \times 5D$ in the axial and radial directions. This calculation was started about five jet diameters upstream of the nozzle exit, with a prescribed inlet turbulence level ($k^{1/2}/U$jet) set at 6% and a length scale of about $0.01D$, in accordance with the European Research Community on Flow, Turbulence and Combustion (ERCOFTAC) guidelines [23].

The unsteady motions in the turbulent jet, that are not present in the RANS calculation but are captured by the LES, are illustrated in Fig. 3 which displays an isosurface of vorticity. This picture shows that the Gaussian noise prescribed at nozzle inlet and the subsequent boundary layer growth predicted on the internal nozzle wall in the current LES prediction do not provide fully turbulent conditions at the nozzle exit lip for initial shear-layer development. These are

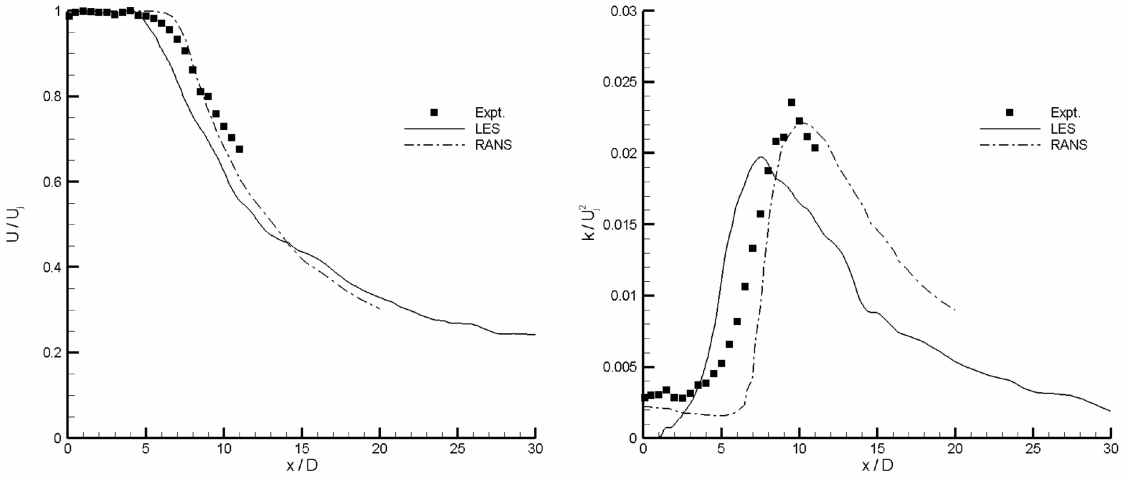

a) Axial velocity **b) Turbulence kinetic energy**

Fig. 5 Centerline variation of axial velocity and turbulence kinetic energy from Power et al. [22].

rather transitional, with vortex rings that break down rapidly into 3D turbulent structures. Radial profiles predicted at $y_1/D = 1$, 5 are shown in Fig. 4. At $y_1/D = 1$ the statistics from both simulations are in good agreement with the experimental data. The LES prediction has a thinner shear-layer than in the RANS solution. At $y_1/D = 5$ the LES somewhat over-predicts the turbulent kinetic energy in the flow. The centerline predictions in Fig. 5 show that the LES also under-predicts the potential core length slightly (Fig. 5a), but is capable of capturing the irrotational fluctuations measured within the potential core (Fig. 5b).

To obtain the temporal-spatial correlation functions from the LES predictions, the flowfields are sampled as described above and are processed using custom-written software developed at the Universities of Loughborough and Cambridge (Hollis [24], de la Rosa Blanco[§§], and Robinson [25]). The 3D unsteady data provided by the LES solution are sampled to provide planes of instantaneous data in a small 2D domain (surrounding any selected point in the flow), which is large enough to cover the spatial separations of interest. The time series of velocity is created by sampling every 40 LES time steps (corresponding to a sampling frequency of ∼50 kHz) and used to determine the two-point two-time products of fluctuating Reynolds stress, and the results were averaged over sample time with the sample size being increased by taking data from other grid planes in the azimuthal (statistically homogeneous) direction. The same methodology was also applied to particle image velocimetry (PIV) data (Pokora and McGuirk [26]) shown in Fig. 6. The second- and fourth-order two-point two-time correlations for the streamwise velocity fluctuations and for a streamwise separation vector (extracted from the LES at a point in the middle of the shear-layer at $y_1/D = 4$) are compared with the hot-wire experimental data of Harper–Bourne [27] and also with PIV measurements by Pokora and McGuirk [26] in Fig. 6. The shape and decay of the curves are in very good agreement with the experimental data. In particular, the agreement of the fourth-order correlation is very encouraging, implying that the current simulation has captured the salient flow physics of the jet turbulence which describe the acoustic sources. It is this information that should prove most useful if it can be incorporated into the acoustic analogy model.

It is encouraging to note that the LES predictions shown in Fig. 6 were based on predictions for a jet of Reynolds number of 10^6 and Mach number of 0.75, whereas the Harper–Bourne [27] experiments were conducted at $Re = 2 \times 10^5$ and $M = 0.18$ and the Pokora and McGuirk [26] PIV data correspond to a water tunnel experiment at $Re = 4 \times 10^4$ and negligible Mach number; this provides some evidence that the correlation shapes are not very sensitive to precise jet flow parameters. This indicates that the source model needed for the acoustic analogy is relatively insensitive to the jet Reynolds and subsonic Mach numbers.

Despite the general very good agreement between the LES results and the correlation measurements, one feature of the latter that is notoriously difficult to predict numerically is the cusps at $\eta_1 = 0$ that are typical of calculations for high-Reynolds-number cases. The true correlations have zero slope at the origin, but the corresponding radius of curvature there is of the order of the Taylor microscale [9,28]. One cannot expect these scales to be resolved in a high-Re LES solution and, consequently, this effect is not included in the model.

To demonstrate the quality of the LES solution used, we have examined the power spectral density of turbulent velocity fluctuations in a typical jet shear location, see Fig. 7. This shows that at this high Re more than one decade of $-5/3$ decay has been captured by the LES at the current grid resolution.

IV. Acoustic Source Modeling and Sound Fields

The fourth-order two-point velocity correlations shown in Fig. 6 have a remarkably simply form. They are well approximated by a Gaussian function of the form

$$R_{ijkl}(\mathbf{y}, \boldsymbol{\Delta}, \tau) = A_{ijkl}(\mathbf{y}) \exp[-\Delta_1/(\bar{u}\tau_s(\mathbf{y})) - \ell n2((\Delta_1 - \bar{u}\tau)^2 + \Delta_2^2 + \Delta_3^2)/l_s^2(\mathbf{y})] \tag{13}$$

Such a function has been used previously [2,14,15], but then it was used to model the sound sources due to fine-scale turbulence. Here we find that the large-scale flow structures captured by the LES have the same form. Comparison of the form in Eq. (13) with the results of the LES simulation also enables us to determine the unknown parameters. In making the comparison in Fig. 8, the values for the amplitude $A_{1111}(\mathbf{y})$, decay time scale $\tau_s(\mathbf{y})$ and Gaussian length scale $l_s(\mathbf{y})$ in Eq. (13) were chosen at each position $\mathbf{x}$ to give the best fit to the LES results. The agreement is encouraging.

Despite the generally very good approximation of the LES data by the Gaussian fits we note a further feature that cannot be approximated using a Gaussian. This concerns the negative loops of the two-point correlation functions. For example, Goldstein and Leib [9] argue that the negative loops are associated with noncompactness effects of large-scale turbulent structures and thus should not be lightly neglected. We believe that it is a straightforward extension of the present approach to use a fitting function that can account for the negative loops, and this will be the subject of future work. In the meantime, we note that the amplitude of the negative loops in the LES solution for most space-time separations is well within 10% of the maximum correlation amplitude. The sensitivity of our current jet noise model to a 10% variation of the various Gaussian fit parameters

[§§]Private communication with E. de la Rosa Blanco, November 2007.

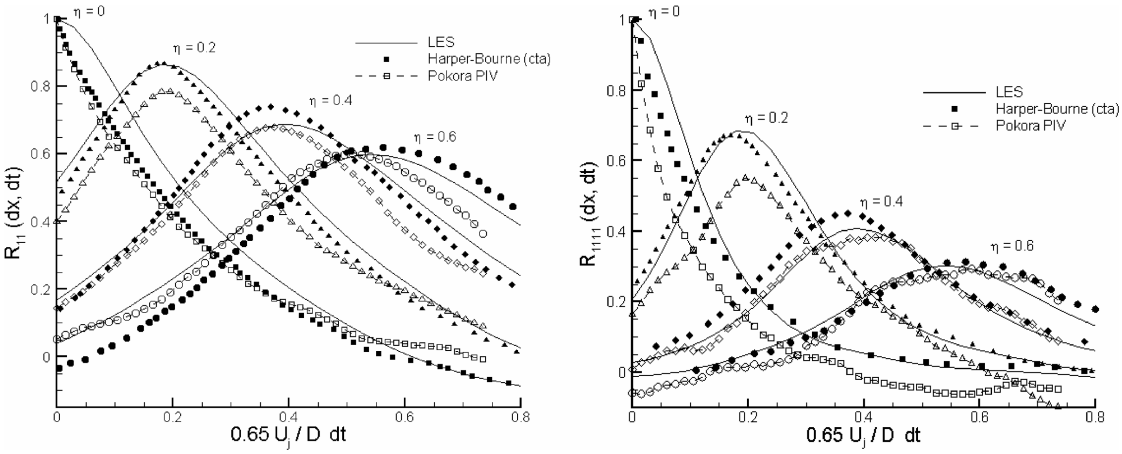

Fig. 6 Comparison between LES predicted correlation functions a) $R_{11}(\mathbf{y}, \mathrm{d}\mathbf{y}, \mathrm{d}t)$ and b) $R_{1111}(\mathbf{y}, \mathrm{d}\mathbf{y}, \mathrm{d}t)$ against Harper–Bourne [27] and Pokora and McGuirk [26] data, at $y_1 = x = 4D$, $y_2 = r = 0.5D$; $\mathrm{d}y_1 = \mathrm{d}x = \eta D$, $\mathrm{d}y_2 = \mathrm{d}y_3 = 0$.

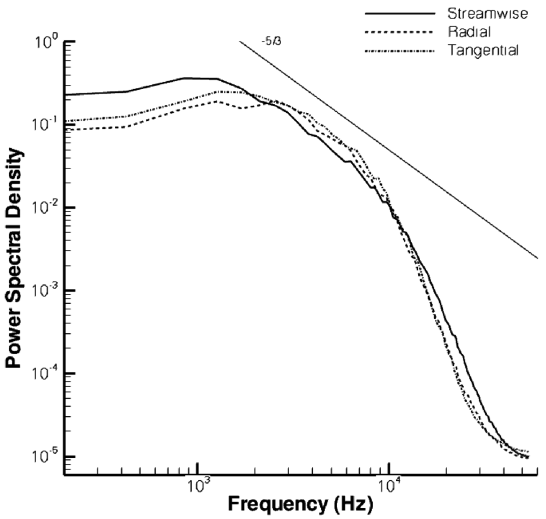

Fig. 7 LES predicted spectra in jet shear layer (lipline) at $x/D = 4.0$.

will be discussed later in the paper, together with the effect on the sound prediction.

The real advantage of using an acoustic analogy lies in its application without recourse to a LES solution. So we investigate to what extent the parameters defining the source statistics, $A_{ijkl}(\mathbf{y})$, $\tau_s(\mathbf{y})$ and $l_s(\mathbf{y})$, can be determined from the much simpler and quicker RANS calculation. One might hope that [10,13–15]

$$A_{ijkl}(\mathbf{y}) = C_{ijkl}(2\bar{\rho}k)^2, \qquad l_s(\mathbf{y}) = c_l k^{3/2}/\varepsilon \quad \text{and} \quad \tau_s(\mathbf{y}) = c_\tau k/\varepsilon \tag{14}$$

where C_{ijlk}, c_l and c_τ are nondimensional constants and $k^{3/2}/\varepsilon$ and k/ε are the usual turbulence length and time scales arising from the RANS calculation.

Figure 9 shows the comparison of the parameters obtained from the best-fit Gaussian with values extracted from the RANS solution. In making the comparison we have plotted the length scale $l_s(\mathbf{y})$ and the autocorrelation time decay constant $\tau_s(\mathbf{y})$. We see that they are proportional to the RANS length and time scales over a wide range of axial positions (from 0.7 to 6 jet diameters D downstream of the nozzle).

Figures 9d–9f shows the comparison of the convection velocity as obtained from the LES data with the local velocity from the RANS solution. The LES convection velocity was determined from the location of the maximum in the fourth-order velocity cross

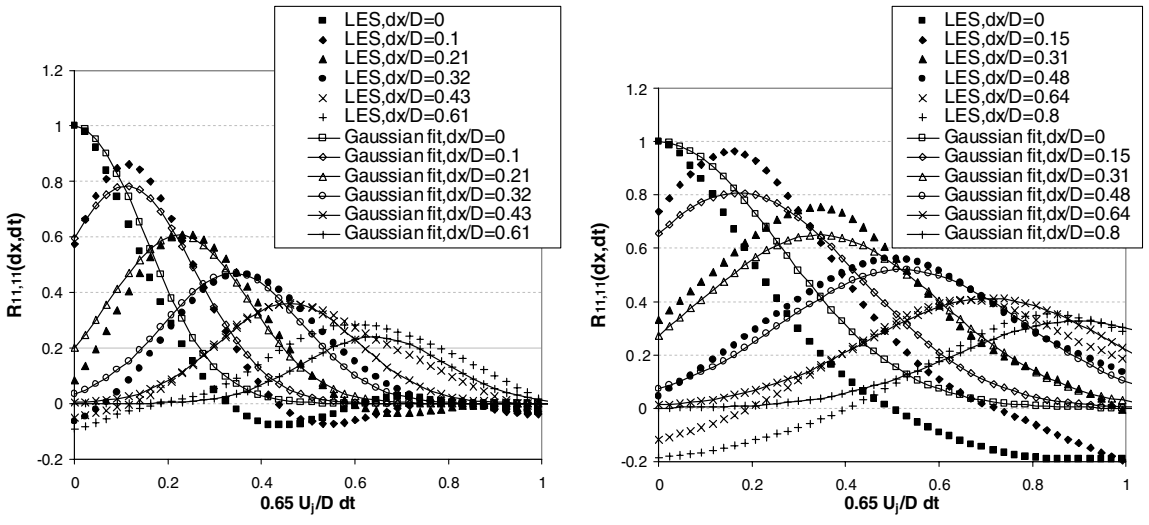

Fig. 8 Gaussian fitting to the LES fourth-order velocity correlation results, which correspond to the shear-layer location $r/D = 0.5$ and two axial locations downstream of the nozzle ($y_1 = 0$) at a) $y_1/D = 4$ and b) $y_1/D = 6$.

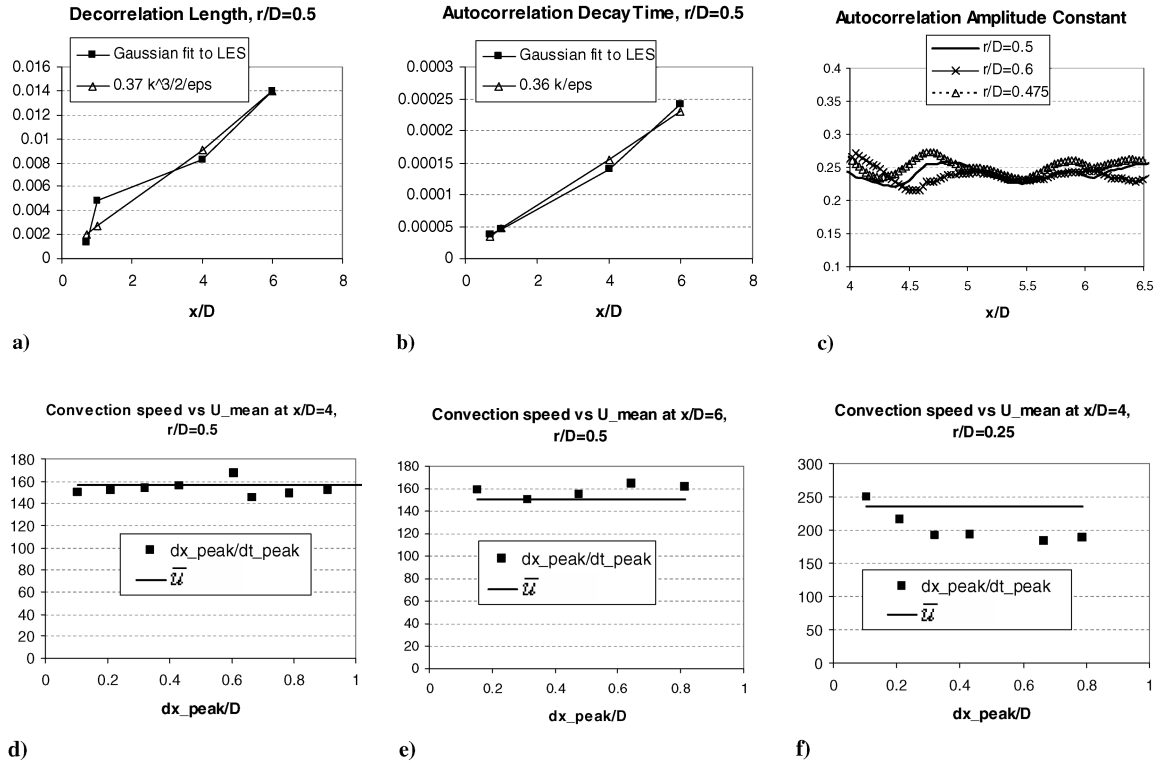

Fig. 9 Axial variation of space, time, and amplitude scales from the best-fit Gaussian to the LES results compared with scales from the RANS for different axial positions downstream of the nozzle ($y_1 = 0$): a) Gaussian length scale $l_s(\mathbf{y})$, b) autocorrelation time decay constant, τ_s, c) $\sqrt{C_{iijj}} = \sqrt{R_{iijj}(\mathbf{y}, \mathbf{0}, 0)}/(2\bar{\rho}k)$, and d–f convection velocity from the LES results at different spatial separations compared with the local flow velocities from the RANS for several locations inside the jet: part d) $y_1/D = 4, r/D = 0.5$, part e) $y_1/D = 6, r/D = 0.5$, and part f) $y_1/D = 4, r/D = 0.25$.

correlations $R_{1111}(\mathbf{y}, \mathbf{dy}, \mathrm{d}t)$ in Fig. 8. The comparison with the local RANS velocity is excellent particularly in the shear layer (Figs. 9d and 9e) and using the local mean RANS velocity in Eq. (13) gives an encouraging fit to the LES (see Fig. 8). Figure 9f shows that the LES convection velocity has more dependence on $\mathrm{d}y_1$ at locations close to the jet axis, but we find later from the contours of contributions to acoustic pressure power spectral density that these regions are not the major contributors to the volume integral that determines the far-field sound.

The fact that the proportionality parameters relating the LES-based length, time, and amplitude scales and the RANS-derived quantities is almost constant is consistent with the findings of Goldstein and Leib [9], who observed that experimental data for the correlation coefficients C_{1111}, c_l and c_τ can be reasonably well represented by the corresponding RANS scales everywhere in the flow. The incorporation of the length scale in the transverse jet direction, which was found to scale less well with the RANS-derived length scale [9], into the current model will also be the subject of future work.

The amplitude comparison is made in Fig. 9c by plotting $\sqrt{C_{iijj}} = \sqrt{R_{iijj}(\mathbf{y}, \mathbf{0}, 0))}/(2\bar{\rho}k)$. Because $R_{iijj}(\mathbf{y}, \mathbf{0}, 0) = \overline{T'_{ii}(\mathbf{y}, t)T'_{jj}(\mathbf{y}, t)}$ this shows the ratio of the square-root of the autocorrelation of T'_{ii} from best-fit Gaussian with the local values of $(2\bar{\rho}k)$ from the RANS. We see that this ratio is approximately constant. The direct proportionality between the best-fit Gaussian values and the RANS parameters means that we can, with confidence, use the RANS results in the description of acoustic sources. The encouraging agreement between the fourth-order velocity correlations and experimental data at different Reynolds and Mach numbers in Fig. 6 strongly suggests that these constants are universal, but until more simulations have been made we cannot say this categorically.

In summary, the relationship between the parameters in the Gaussian that gives the best fit to the LES and the RANS scales are

$$c_l = 0.37, \qquad c_\tau = 0.36 \quad \text{and} \quad \sqrt{C_{iijj}} = 0.25 \tag{15}$$

They are compared with values used in the literature [12,13] based on best fits to the far-field sound in Table 1.

In the comparison in Fig. 9c, we have just plotted $\sqrt{C_{iijj}}$, but we can also use the LES solution to determine the relative magnitudes of all the components of R_{ijkl}. Analysis of the LES solution shows that the only significant components are R_{1111}, R_{2222} and R_{3333} (where the Cartesian directions are defined as one being the jet flow direction and two and three being in the cross plane, corresponding to the circumferential and radial directions, respectively, at this location) and the cross terms R_{1212}, R_{1313}, and R_{2323} (and the terms they are equal to by symmetry, such as R_{2112}, R_{1221} etc.). Moreover their relative magnitudes are remarkably independent of position $\mathbf{x}$ within the jet (see Fig. 10). Having informed the choice of the nondimensional constants of proportionality through comparison with the LES solution, there are no remaining undetermined empirical constants in the source description and we can obtain absolute predictions for the sound field. While symmetric source descriptions have been used previously [9,29,30] within an acoustic analogy, here the relative magnitudes of the different components are determined from analysis of the fourth-order velocity cross correlations in the LES results rather empirically or through ad hoc assumptions.

In Figs. 11–14, we present results for the sound field predicted using the source description in Eqs. (13–15) for the jet in the JEAN project [22], and compare these predictions with experimental results obtained in that project. The propagation through the jet emerging from a nozzle is described by the adjoint Green function and is determined through the numerical solution of the system of LEEs

Table 1 Nondimensional time, length, and amplitude constants

Nondimensional constants	Tam and Auriault [14]	Morris and Farassat [15]	Current prediction based on LES
Space scale, c_l	0.13	0.78	0.37
Time scale, c_τ	0.308	1	0.36
Amplitude scale, $\sqrt{C_{iijj}}$	0.257	0.26	0.25

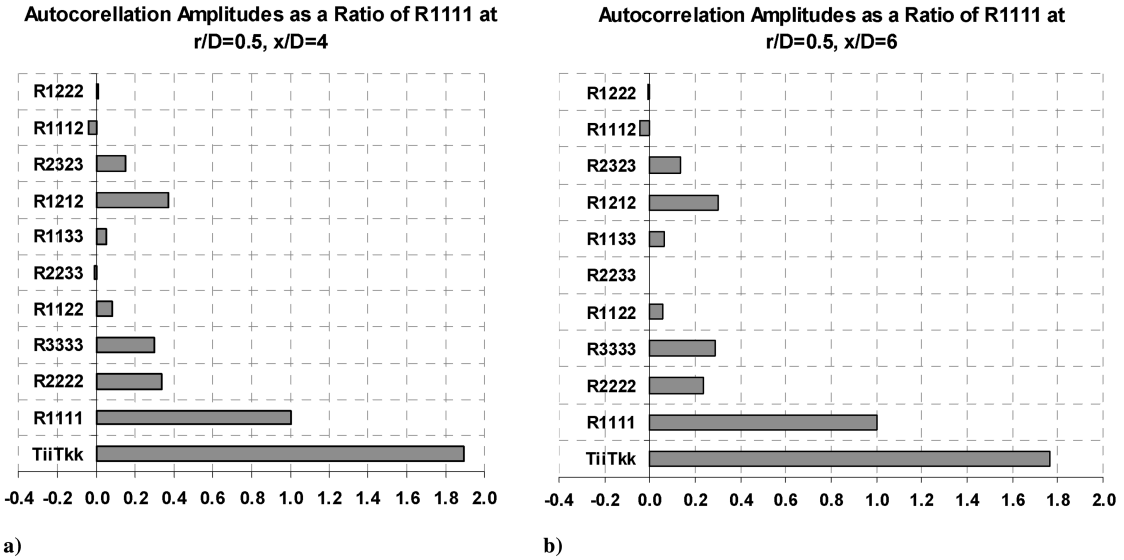

Fig. 10 Autocorrelation amplitudes as a ratio of $R_{1111}(\mathbf{x}, 0, 0)$ in the shear-layer location $r/D = 0.5$; downstream of the nozzle ($y_1 = 0$) at a) $y_1/D = 4$ and b) $y_1/D = 6$. The data is presented for an azimuthal location for which the two directions of the Cartesian coincides with the local circumferential direction and the three with the local radial.

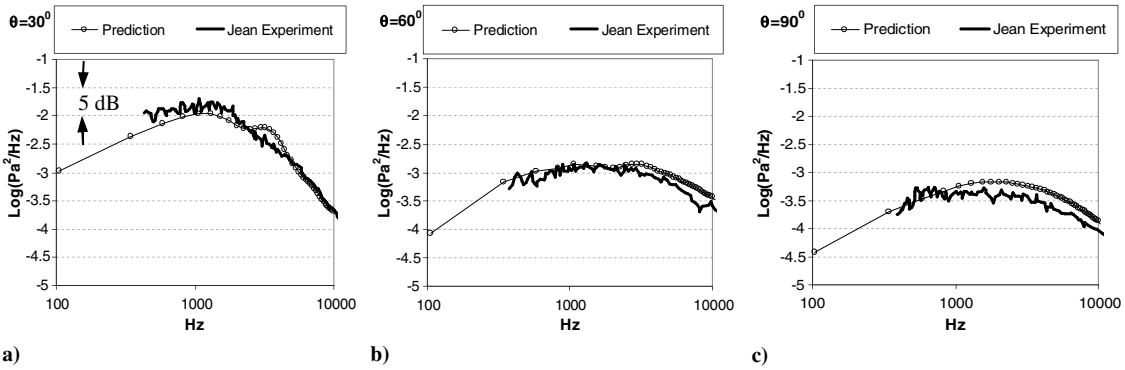

Fig. 11 Spectra comparison with experiment at a) 30°, b) 60°, and c) 90° to the jet axis for predictions based on a Green function for a spreading jet mean flow and the Gaussian source model informed by the LES.

described in Sec. II and includes scattering by the nozzle and jet spreading. The mean flow is taken from the RANS solution.

A very good sound prediction is obtained that, as shown in Fig. 11, is within 2 dB of the experimental data for all angles. This is the main result of this paper. In these plots a frequency of 5 kHz corresponds to a Strouhal number of 1. It should be emphasized that there are no empirical constants in the description of the acoustic source terms, which are determined from the RANS solution with constants of proportionality fixed entirely using data extracted from the near-field LES results. Although only the main source components have been included in these plots ($R_{1111}, R_{2222}, R_{3333}, R_{1212}, R_{1313}$ and R_{2323} (and terms equal to these from symmetry) the remaining terms are so small that there is no difference in the predicted spectrum if all source components are included with their relative amplitudes as determined from the LES results.

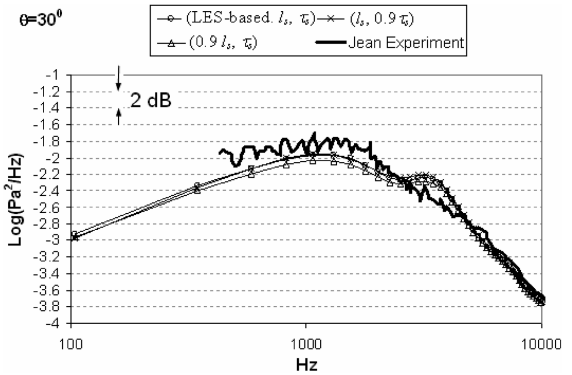

Fig. 12 Sensitivity of the power spectral density predictions shown in Fig. 11a to a 10% variation of the LES-derived length ($0.9l_s, \tau_s$) and time ($l_s, 0.9\tau_s$) correlation scales. The original solution based on the LES-derived scales (LES-based. l_s, τ_s) is shown for comparison.

To further investigate the sensitivity of the predicted sound to model parameters, the same calculations have been repeated with separate variations of the length and time scale parameters of the Gaussian fit, as defined in Eqs. (13) and (14), with l_s and τ_s reduced by 10% from the best-fit values obtained from the LES solution. The results show that in all cases the resulting computed sound spectral density remains the same to within 0.2–0.7 dB and is within the 2 dB errorband of the experimental data for all frequencies (Fig. 12). This appears to confirm that the acoustic model used remains fairly robust to reasonable variations in the parameters used in the Gaussain fits to the LES data.

One advantage of deriving the sound field through a representation theorem as in this paper is that, because the far-field sound is obtained by integrating the product of the Green function and the source, it is possible to identify the jet locations that contribute most to the sound at different frequencies. Sample results are shown in Figs. 13 and 14, normalized by the peak sound intensity at the small angle to the jet. As expected, as the frequency increases, the most significant sound producing zone in the jet moves upstream toward the nozzle exit. For angles close to the jet and the peak sound frequency $St = 0.2$, the most significant source location is a region seven to 14 diameters

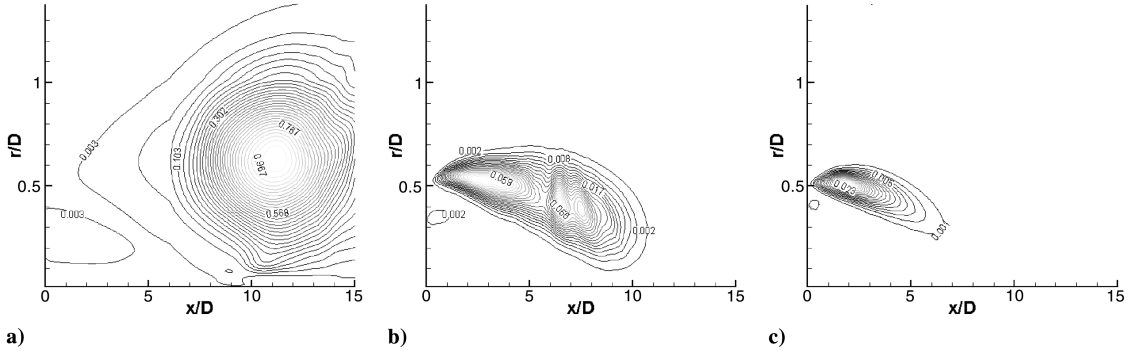

Fig. 13 Contours of contributions to acoustic pressure power spectral density, i.e., the inner convolution product of the propagation operator based on the Green function and the source function based on the Gaussian source description informed by LES, normalized by the peak sound value for the observer location at 30° to the jet, which demonstrate locations in the jet that contribute most to the sound spectra at different frequencies: a) $St = 0.2$ (peak sound), and b) $St = 1$ (c) $St = 2$.

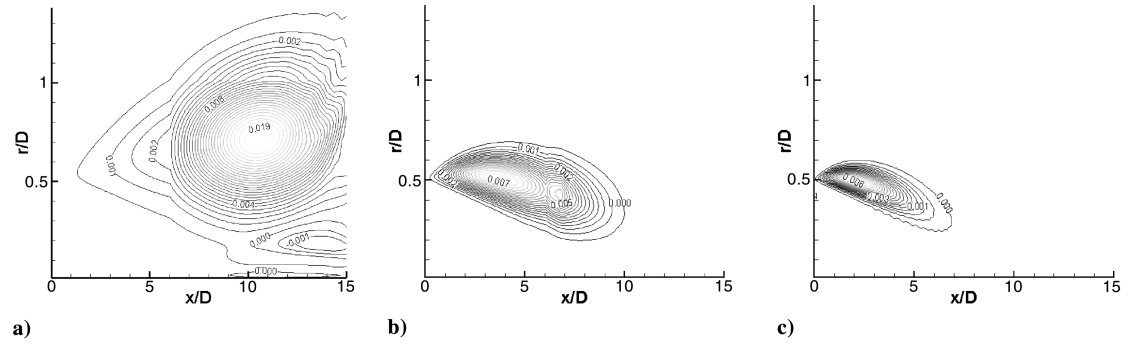

Fig. 14 As Fig. 13 but for an observer location at 90° to the jet.

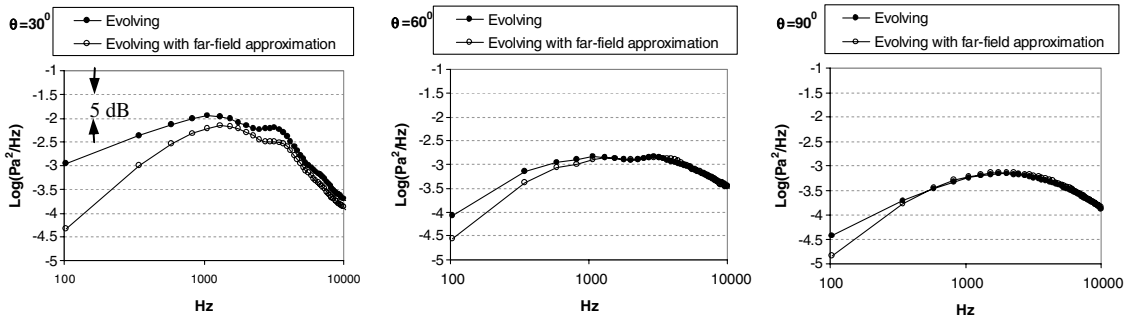

Fig. 15 Effect of the far-field approximation in the Green function on the predicted sound field at $R = 30D$, comparing the solutions obtained from retaining only the leading term (far-field approximation) and the first two terms in the small D/R expansion of the Green function as described in Sec. II at a) 30, b) 60, and c) 90° to the jet axis.

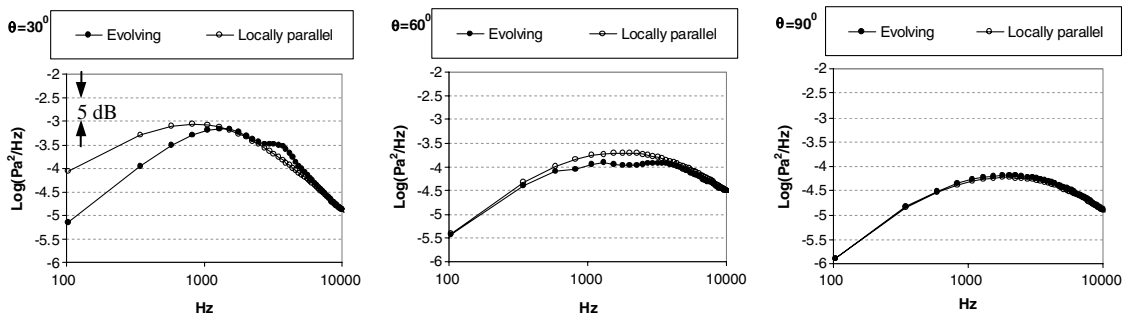

Fig. 16 Comparison of spectra at a) 30, b) 60, and c) 90° to the jet axis and $R = 100D$ for predictions based on the spreading mean-flow jet Green function and on a locally parallel mean flow.

downstream of the nozzle in the shear layer. Although the contours for an observer position at 90° to the jet axis (Fig. 14) look similar in shape to those in Fig. 13, the relative levels at different Strouhal numbers are significantly different: at 90° the sound has a much broader spectrum and its peak is moved to $St \sim 0.4$ ($f \sim 2000$ Hz), as indicated in Fig. 11c.

For this source model, we have tested a few commonly made approximations. Firstly, we note that in the JEAN experimental project [22], the acoustic measurements were made at a radius $R = 30D$ from the nozzle exit, which turns out to be sufficiently close to the jet so that a near-field correction should be retained in the free-space Green function. This can be seen from Fig. 15 which compares the predicted sound spectra using just the first term in the far-field expansion of the Green function with predictions when the next term in D/R is also included as described in Sec. II and used in Fig. 11. For example, using the far-field form at a radius $R = 30D$ would result in a an underprediction of the 30° spectrum (Fig. 15a) of about 2–3 dB for peak sound and may be as large as 12–13 dB at low frequencies.

We also study the effect of the mean-flow propagation model on the sound prediction. Figure 16 shows comparison between predictions obtained using the Green function for a spreading jet mean flow, which includes scattering by the nozzle, with those using a Green function based on a locally parallel mean-flow approximation. The parallel mean-flow Green function can be calculated by a semi-analytic method requiring the numerical solution of an ordinary differential equation, but only for a far-field observer. Hence, the comparison between the propagation models is made for an observer located at 100 jet diameters from the nozzle exit, at which distance the far-field approximation was checked to be appropriate. We note that while both models capture the propagation effects at sideline (90° to the jet), the locally parallel jet approximation overpredicts the sound near the jet axis. At angles near the jet, a small local maximum near 6 kHz is predicted. This may be due to nozzle scattering because the nozzle diameter is then half a wavelength. There is no similar peak in the measured spectrum and thus this may be a numerical artifact.

It is worth comparing the shapes of the predicted spectra at 30 and 90° with the similarity spectra proposed by Tam et al. [31]. These spectra have been derived, separately for small and large observer angles, by Tam et al. [32] after an extensive postprocessing of a large amount of experimental data contained in a NASA database. The empirical functions corresponding to high and small observer angles to the jet are referred to as the broadband (G) and narrowband (F) spectrum, respectively. According to the two-source jet noise hypothesis of Tam et al. [31] the two empirical spectra are attributed to the fine-scale and large-scale mechanisms of mixing noise, with the large-scale noise generation mechanism dominant at small observer angles and the small-scale dominant at 90°.

Figure 17 shows the experimental data and the predicted far-field spectra solutions collapsed to G and F shapes and compared with the original G and F functions digitized from Tam et al. [31]. Following Tam et al. [31], in order to collapse to the canonical G and F shapes all spectral data have been first normalized by the peak sound pressure spectral density values and then plotted as functions of a nondimensional parameter f/f_0, where f is the dimensional frequency and f_0 is the peak frequency. It can be seen that the

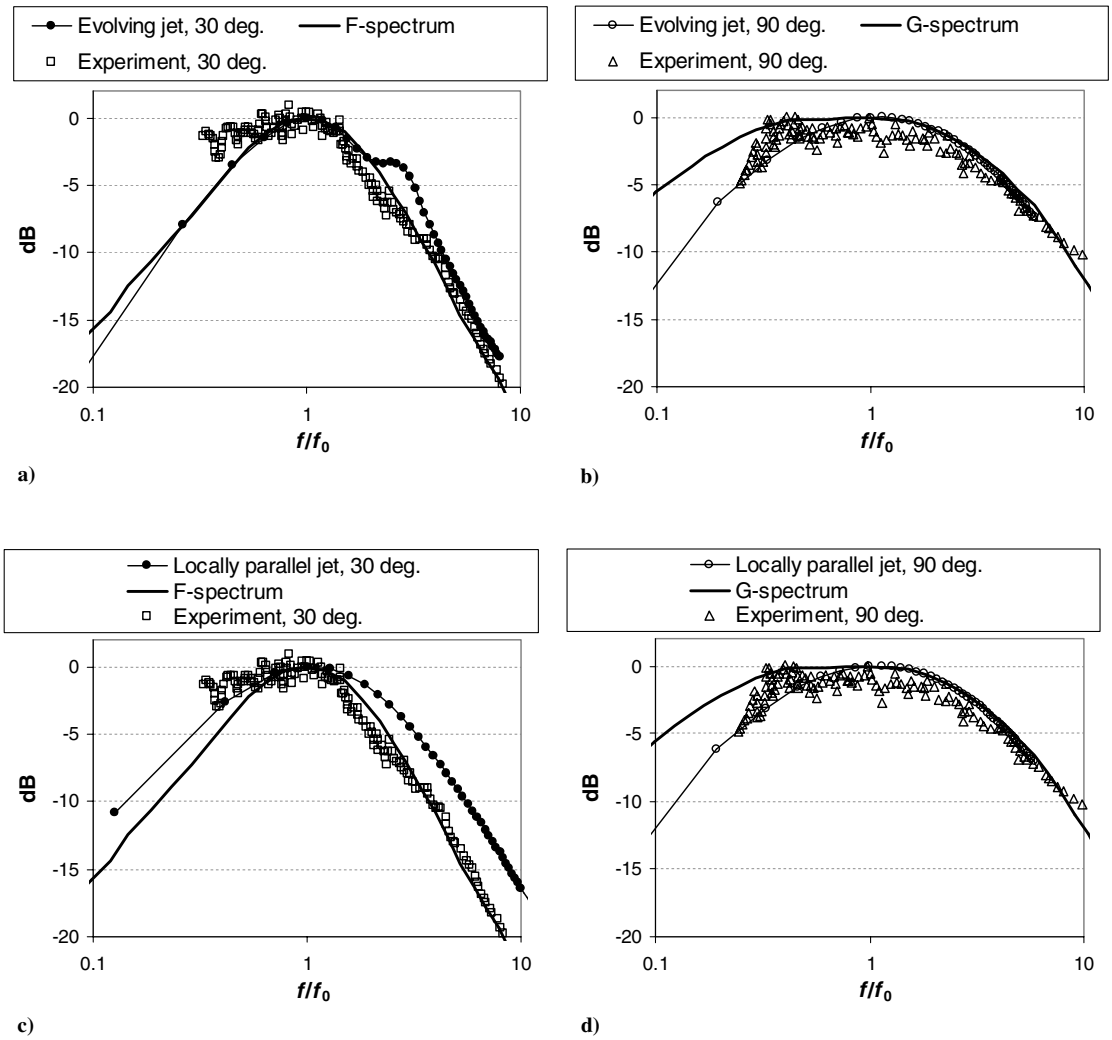

Fig. 17 Comparison of the similarity spectra of Tam et al. [32] and the scaled JEAN experiment data. Parts a and b show spreading jet prediction at $R = 100D$. Parts c and d show locally parallel jet prediction.

similarity sound spectra do, indeed, provide a good fit to the measurements, except for the low-frequency part of the spectrum. For a wide range of frequencies, the agreement between the spreading jet solution with the experiment and the reference F-spectrum, and G-spectrum is within 1–2 dB.

Also shown in Figs. 17c and 17d are the predictions using a locally parallel jet solution to the LEE. The agreement with the experiment and the reference spectra are also good for the 90° observer location, but at 30° when the propagation effects are more important, the locally parallel solution diverges from reference F-spectrum by 5–6 dB at high frequencies. We also note that the observed loss of accuracy of the present locally parallel jet model in comparison with the fully spreading jet solution and the experiment for the observer location at 30° to the jet axis is similar to the 3–4 dB error of the weakly nonparallel jet solution of Goldstein and Leib (figure 6e in [9]) for high frequencies ($St \sim 1$–2) for a similar isothermal, $M = 0.9$ jet.

The final part of this section explores various common approximations made during the evaluation of the source integrals and simplifications of the turbulent acoustic source model. In Fig. 18, we test the error introduced by assuming that the radial variations of the Green function and its derivatives in I_{ij} defined in Eq. (10) are small over the correlation length of the turbulent sources, an approximation made by Tam and Auriault [14] and others. The comparison is made for the full spreading jet propagation model including the nozzle effect and for the same observer distance $R = 30D$ as in the JEAN project test data. The source involves a shear term T'_{13} (3 is in the radial direction), which is multiplied by a propagation term $\partial G_1/\partial r$, and because the axial velocity-like variable in the Green function, G_1, varies rapidly with radius in the shear layer it and its derivative are not necessarily negligible over a turbulent correlation length. The effect of these approximations is particularly drastic at low frequencies where the shear source terms [9,16] are important in the source model (Figs. 18a and 18b).

So far in this work our the source directivity has been informed by the relative magnitudes of the different components provided by the LES solution. Without such information, it has been common to assume source isotropy [14,16]. Results for isotropic sources and a

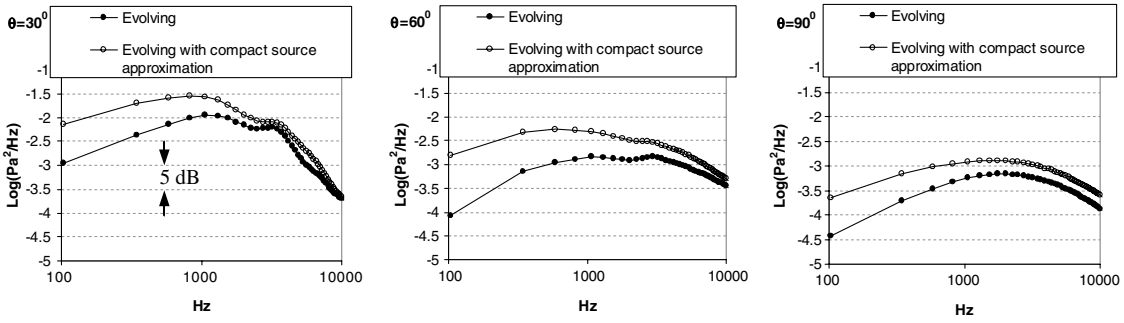

Fig. 18 The effects of neglecting of the radial variation of the Green function over the correlation length of the turbulent sources on spectra at a) 30, b) 60, and c) 90° to the jet axis for $R = 30D$.

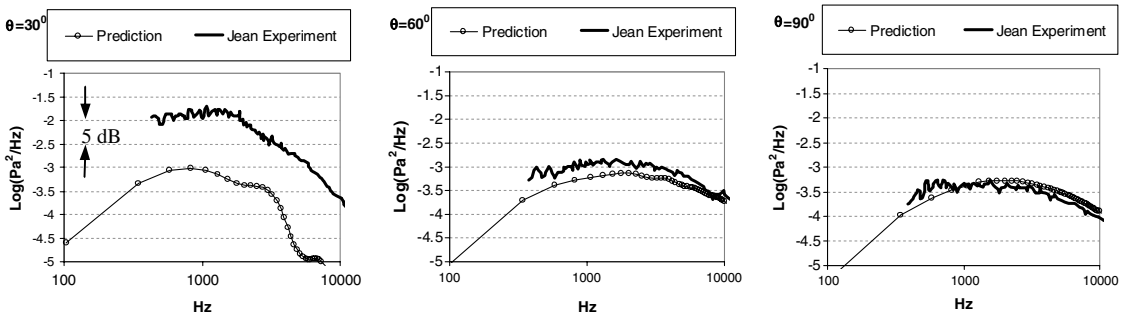

Fig. 19 Spectra comparison with experiment at a) 30, b) 60, and c) 90° to the jet axis for predictions based on the spreading jet mean-flow model and the instantaneously isotropic source model based on $R_{ijkl} = R_{ppqq}\delta_{ij}\delta_{kl}/9$.

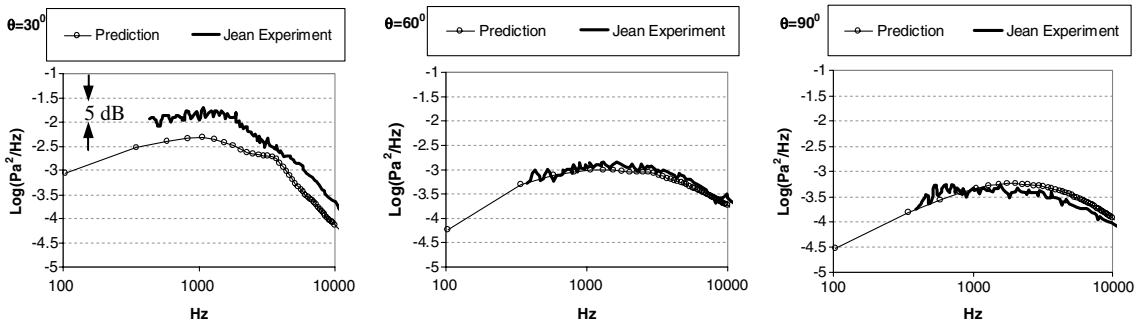

Fig. 20 Spectra comparison with experiment at a) 30, b) 60, and c) 90° to the jet axis for predictions based on the spreading jet mean-flow model and the statistically isotropic source model based on $R_{ijkl} = R_{ppqq}(\delta_{ij}\delta_{kl} + \delta_{ik}\delta_{jl} + \delta_{il}\delta_{jk})/15$.

Green function based on the spreading jet emerging from a nozzle are shown in Figs. 19 and 20. Firstly, a simple instantaneously isotropic model of turbulence is used as in [15]. In this source model $R_{ijkl}(\mathbf{y})$ is taken to be proportional to $\delta_{ij}\delta_{kl}$. We can write the constant of proportionality in the form

$$R_{ijkl}(\mathbf{y}) = R_{ppqq}\delta_{ij}\delta_{kl}/9 \tag{16}$$

In making this comparison of the sound field, we have matched $R_{ppqq}(\mathbf{y})$ to the LES results by using Eqs. (13) and (14) with $\sqrt{C_{ppqq}} = 0.25$. The results are shown in Fig. 19. This gives reasonable predictions at 90° to the jet axis but leads to a major underprediction at small angles to the jet. It should be recognized that the amplitude level in this prediction is somewhat arbitrary because the source direction is not modeled correctly. If instead of matching $R_{ppqq}(\mathbf{y})$, we had matched $R_{1111}(\mathbf{y})$ all predictions would have been 7 dB higher with their shape and relative levels unchanged. Assuming statistical isotropy (i.e., $R_{ijkl}(\mathbf{y})$ proportional to $\delta_{ij}\delta_{kl}+\delta_{ik}\delta_{jl}+\delta_{il}\delta_{jk}$) leads to some improvement in sound prediction but the peak noise spectral levels still remain some 5 dB underestimated (Fig. 20). The results in Fig. 10 show clearly the anisotropy in the acoustic sources and so we should not be surprised that the sound fields predicted from the isotropic source models in Figs. 19 and 20 are unable to capture the sound correctly.

V. Conclusions

We have developed a simple prediction methodology for jet noise. The approach is a hybrid one made up of three components, with each component using modeling and numerical techniques optimized to suit a particular purpose. The propagation of noise to the far field is captured via a solution of the adjoint LEE to determine the adjoint Green function describing how sound emitted by the jet is modified by propagation through the time-averaged but spatially developing jet flowfield. The sound generation is described by Goldstein's acoustic analogy. A Gaussian function is used to model the cross correlation of the fourth-order velocity fluctuations which are the main acoustic sources in an isothermal jet, and the parameters describing their amplitude, length and time scales are taken to be proportional to the local square of the kinetic energy, the length and timescales from a RANS solution. We have determined the constants of proportionality through comparison with correlations obtained from LES. Comparison has also been made with experiments for unheated, moderate Mach number jets at different Reynolds numbers and the constants appear to be universal for this class of jet. If this is the case, only a single LES calculation is needed to predict the noise of simple subsonic isothermal round jets although additional LES calculations would be required to extend this approach to other configurations such as coaxial jets or a chevron nozzle or to heated and higher Mach number jets.

The LES results have been used to determine the relative magnitudes of the various components of the acoustic sources and only a few terms are found to be significant. The fourth-order correlation of the axial velocity R_{1111} is approximately 3 times R_{2222} and R_{3333}, and the radial component R_{3333} tends to be slightly larger than the circumferential term R_{2222}. In addition to these components, R_{1212}, R_{1313} and R_{2323} (and the components they are equal to by the symmetry) are also significant. The ratio of the relative magnitude of the various components in the source is found not to change with position in the jet. Thus informed by the LES solution, the source description is determined with no empirical constants. The far-field sound is then predicted through an integration of the Green function with this acoustic source. Comparison between this predicted noise and the JEAN [20] experimental data gives encouraging agreement across a wide spectral range, even at angles close to the jet axis. Additional checks have confirmed that for all frequencies and observer angles the sound predictions obtained remain the same within 0.2–0.7 dB for variations of the order of 10% in the Gaussian fit parameters based on the LES data. Investigation of the integrand determines the regions of the jet that contribute most to the sound field at different frequencies and observer positions.

We have used the methodology to determine the accuracy of some commonly made approximations. These include:

Effect of Jet Evolution and Scattering by the Nozzle on the Sound Propagation at Shallow Angles to the Jet: This was determined by comparison of results using a numerically determined Green function with results calculated analytically for a locally parallel mean flow for a far-field observer location at $R/D = 100$. In the example considered of a 0.75 M number isothermal jet, it led to a difference up to 10 dB at very low frequencies. The results predicted here for sound at 30° an 90° to the jet are, except at low frequencies, in agreement with general form of the F and G-spectra of Tam et al. [31]. Making a locally parallel jet assumption to model the propagation leads to the differences with the measure spectra that are as large as 5–6 dB at $St \sim 1$–2, confirming the importance of capturing mean-flow sound propagation effects at small angles to the jet.

Isotropic Source Models Used Previously in the Literature: We have found significant differences in the far-field sound according to the assumed relative values of the components of the turbulent sources Analysis of the LES results has shown that the sources are far from isotropic. However, only a few components are significant and their ratios as determined from the LES results appear to be independent of position in the jet. When the ratio of components from the LES solution is used in the source description the predicted sound agrees well with experimental data for all frequencies and angles.

Assumption that the Radial Variation of Green Function is Small over the Correlation Length of the Turbulent Sources: When the sources have nonzero shear terms, e.g., T'_{13} is nonzero, the propagation terms involve the radial derivative of the axial adjoint velocity variable. This varies rapidly across the shear layer of the jet boundary and cannot be assumed to be uniform across the correlation length of the turbulent sources. To assume that it is can lead to errors of in excess of 6 dB at shallow angles to the jet.

Far-Field Form: For the experimental data set we were using, the experimental data at $R/D = 30$ is sufficiently close to the jet that making a far-field approximation in the Green function leads to large errors in the spectral density for mid and low frequencies at angles close to the jet (for example, an error of 2–3 dB at 1 kHz and 12–13 dB at 100 Hz for $\theta = 30°$) where the acoustic wavelengths are about the same or even larger than the distance of the measurement position from the nozzle exit. The near field correction should be included in the calculation of the Green function.

Acknowledgments

This research was funded by the Engineering and Physical Sciences Research Council, and carried out in collaboration with Rolls-Royce, plc. Their support and interest is gratefully acknowledged. The work of S. A. Karabasov has been supported by the Royal Society of London. The RANS calculations were performed by Olivier Marsden, and Elena de la Rosa Blanco helped with the analysis of the large eddy simulation results.

References

[1] Lighthill, M. J., "On Sound Generated Aerodynamically: I. General Theory," *Proceedings of the Royal Society of London, Series A: Mathematical and Physical Sciences*, Vol. 211, No. 1107, 1952, pp. 564–587. doi:10.1098/rspa.1952.0060

[2] Ffowcs Williams, J. E., "The Noise From Turbulence Convected at High Speed," *Philosophical Transactions of the Royal Society of London*, Vol. 255, No. 1061, 1963, pp. 469–503.

[3] Dowling, A. P., Ffowcs Williams, J. E., and Goldstein, M. E., "Sound Production in a Moving Stream," *Philosophical Transactions of the Royal Society of London, Series A: Mathematical and Physical Sciences*, Vol. 288, No. 1353, 1978, pp. 321–349. doi:10.1098/rsta.1978.0019

[4] Mani, R., "The Influence of Jet Flow on Jet Noise," *Journal of Fluid Mechanics*, Parts 1 and 2, Vol. 73, 1976, pp. 753–793. doi:10.1017/S0022112076001602

[5] Lilley, G. M., "On the Noise from Jets," *Noise Mechanisms*, Agard CP-131, 1974, 113.1–13.12.

[6] Colonius, T., Lele, S. K., and Moin, P., "Sound Generation in a Mixing Layer," *Journal of Fluid Mechanics*, Vol. 330, 1997, pp. 375–409. doi:10.1017/S0022112096003928

[7] Goldstein, M. E., "A Generalized Acoustic Analogy," *Journal of Fluid Mechanics*, Vol. 488, 2003, pp. 315–333. doi:10.1017/S0022112003004890

[8] Samanta, A., Freund, J. B., Wei, M., and Lele, S. K., "Robustness of Acoustic Analogies for Predicting Mixing-Layer Noise," *AIAA Journal*, Vol. 44, No. 11, Nov. 2006, pp. 2780–2786. doi:10.2514/1.22186

[9] Goldstein, M. E., and Leib, S. J., "The Aeroacoustics of Slowly Diverging Supersonics Jets," *Journal of Fluid Mechanics*, Vol. 600, 2008, pp. 291–337.

[10] Tam, C. K. W., and Auriault, L., "Mean Flow Refraction Effects on Sound Radiated from Localized Sources in a Jet," *Journal of Fluid Mechanics*, Vol. 370, 1998, pp. 149–174. doi:10.1017/S0022112098001852

[11] Argawal, A., Morris, P. J., and Mani, R., "Sound Propagation in Non-Uniform Flows: Suppression Of Instability Waves," *AIAA Journal*, Vol. 42, No. 1, 2004, pp. 80–88. doi:10.2514/1.619

[12] Karabasov, S. A., and Hynes, T. P., "Adjoint Linearized Euler Solver in the Frequency Domain for Jet Noise Modeling," *12th AIAA/CEAS*, AIAA Paper 2006-2673, Cambridge, MA, 2006.

[13] Bechara, W., Lafon, P., Bailly, C., and Candel, S. M., "Application of a k-ε Turbulence Model to the Prediction of Noise for Simple and Coaxial Free Jets," *Journal of the Acoustical Society of America*, Vol. 97, No. 6, 1995, pp. 3518–3531. doi:10.1121/1.412438

[14] Tam, C. K. W., and Auriault, L., "Jet Mixing Noise from Fine Scale Turbulence," *AIAA Journal*, Vol. 37, No. 2, 1999, pp. 145–153.

[15] Morris, P. J., and Farassat, F., "Acoustic Analogy and Alternative Theories for Jet Noise Prediction," *AIAA Journal*, Vol. 40, No. 4, 2002, pp. 671–680. doi:10.2514/2.1699

[16] Afsar, M. Z., Dowling, A. P., and Karabasov, S. A., "Jet Noise in the Zone of Silence," *13th AIAA/CEAS Aeroacoustics Conference*, AIAA Paper 2007-3606, May 2007.

[17] Bogey, C., and Bailly, C., "Computation of a High Reynolds Number Jet and its Radiated Noise Using Large Eddy Simulation Based on Explicit Filtering," *Computers and Fluids*, Vol. 35, No. 10, 2006, pp. 1344–1358. doi:10.1016/j.compfluid.2005.04.008

[18] Andersson, N., Eriksson, L. E., and Davidson, L., "Investigation of an Isothermal Mach 0.75 Jet and its Radiated Sound Using Large-Eddy Simulation and Kirchhoff Surface Integration," *International Journal of Heat and Fluid Flow*, Vol. 26, No. 3, 2005, pp. 393–410. doi:10.1016/j.ijheatfluidflow.2004.09.004

[19] McMullan, W. A., Pokora, C. D., Page, G. J., and McGuirk, J. J., "Large Eddy Simulation of a High Reynolds Number Subsonic Turbulent Jet for Acoustic Source Capture," *14th AIAA/CEAS Aeroacoustics Conference*, AIAA Paper 2008-2974, May 2008.

[20] Page, G. J., Zhao, H., and McGuirk, J. J., "A Parallel Multi-Block Reynolds-Averaged Navier–Stokes Method for Propulsion Installation Application," *12th International Symposium on Air Breathing Engines*, Vol. 1, AIAA, Washington, D. C., 1991, pp. 864–876.

[21] Page, G. J., Li, Q., and McGuirk, J. J., "LES of Impinging Jet Flows Relevant to Vertical Landing Aircraft," *23rd AIAA Applied Aerodynamics Conf.*, AIAA Paper 2005–5226, June 2005.

[22] Power, O., Kerherve, F., Fitzpatrick, J., and Jordan, P., "Measurements of Turbulence Statistics in High Subsonic Jets," *10th AIAA/CEAS Aeroacoustics Conference*, AIAA Paper 2004-3021, June 2004.

[23] ERCOFTAC Special Interest Group on Quality and Trust in Industrial CFD, Best Practice Guidelines 1999.

[24] Hollis, D., "Particle Image Velocimetry in Gas Turbine Combustor Flowfields," Ph.D. Thesis, Loughborough University, Loughborough, England, 2004.

[25] Robinson, M. D., "Unsteady Inlet Condition Generation for Large Eddy Simulation CFD Using Particle Image Velocimetry," Ph.D. Thesis, Loughborough University, Loughborough, England, 2009.

[26] Pokora, C., and McGuirk, J. J., "Spatio-Temporal Turbulence Correlations Using High-Speed PIV in an Axisymmetric Jet," *14th AIAA/CEAS Aeroacoustics Conference*, AIAA Paper 2008-3028, May 2008.

[27] Harper–Bourne, M., "Jet Noise Turbulence Measurements," *9th AIAA/CEAS Aeroacoustics Conference*, AIAA Paper 2003-3214, 2003.

[28] Pope, S. B., *Turbulent Flows*, Cambridge Univ. Press, Cambridge, England, 2008.

[29] Kraichnan, R. H., "Pressure Field Within Homogeneous Anisotropic Turbulence," *Journal of the Acoustical Society of America*, Vol. 28, No. 1, 1956, pp. 64–72. doi:10.1121/1.1908224

[30] Goldstein, M. E., and Rosenbaum, B., "Effect of Anisotropic Turbulence on Aerodynamic Noise," *Journal of the Acoustical Society of America*, Vol. 54, No. 3, 1973, pp. 630–645. doi:10.1121/1.1913643

[31] Tam, C. K. W., Viswanathan, K., Ahuja, K. K., and Panda, J., "The Sources of Jet Noise: Experimental Evidence," *Journal of Fluid Mechanics*, Vol. 615, 2008, pp. 253–992. doi:10.1017/S0022112008003704

[32] Tam, C. K. W., Golebiowski, M., and Seiner, J. M., "Two Components of Turbulent Mixing Noise from Supersonic Jets," AIAA Paper 96–1716, 1996.

C. Bailly
Associate Editor